CLM-P855

CLM-P855

Multiphase Detonation Modelling using the CULDESAC Code

D. F. Fletcher A. Thyagaraja

UK ATOMIC ENERGY AUTHORITY

Culham Laboratory

CLM-P855

Multiphase Detonation Modelling using the CULDESAC Code

D.F. Fletcher and A. Thyagaraja

Culham Laboratory, Abingdon, Oxon., OX14 3DB

ABSTRACT

In this paper we describe a mathematical model of melt/water detonations. This model has been developed to study the escalation and propagation stages of a vapour explosion. After describing the physics of this problem we give a complete description of the conservation equations and constitutive relations which form the model. We then describe the the solution procedure and present some results from simulations which have been performed in order to study the effect of the presence of permanent gas in the coarse mixture and to compare our predictions using an approximate EOS with those using a standard steam table package.

Submitted for presentation at the 12th International Colloquium on the Dynamics of Explosions and Reactive Systems (ICDERS) to be held at the University of Michigan, 23-28 July, 1989.

December, 1988

Contents

Nomenclature

A	area factor
c_d	drag coefficient
c_{frag}	constant in the fragmentation model
c_v	specific heat at constant volume
e	internal energy
e_s	stagnation energy
h	heat transfer coefficient
h_s	stagnation enthalpy
K	momentum exchange function
L	length-scale
p	pressure
R	energy exchange function
T	temperature
t	time
V	velocity
X	approximation to α_w in the iteration scheme
x	axial coordinate or mass quality

Greek Symbols

α	volume fraction or void fraction
ρ	density
ν	specific volume ($= 1/\rho$)
γ	ratio of specific heats
Γ_f	mass transfer rate
Γ_{frag}	length-scale source term
Γ_v	Grüneisen coefficient
Δt	space step
Δx	time step

Subscripts

e	effective fluid (water plus fragments and gas)
f	fragments
g	gas
liq	saturated liquid
m	melt droplets
sat	saturation value
vap	saturated vapour
w	water

1 Introduction

If a hot liquid (melt) contacts a cooler volatile liquid, in some circumstances the energy transfer rate can be so rapid and coherent that an explosion results. Such explosions are a well-known hazard in the metal casting industry [1] and it is postulated that they may occur in submarine volcanisms [2]. They are also studied in the nuclear industry, to assess the consequences of the unlikely event that in a severe accident molten material contacts residual coolant and such an explosion results [3].

Explosions of this type are known to progress through a number of distinct phases [3]. Initially, the melt and water mix on a relatively slow timescale (~1 second). During this stage the melt and water zones have a characteristic dimension of the order of 10mm. Because of the high temperature of the melt, a vapour blanket insulates the melt from the water and there is relatively little heat transfer. If this vapour blanket is collapsed in some small region of the mixture, high heat transfer rates result and there is a rapid rise in the pressure locally. In some circumstances this pressure pulse can cause further vapour film collapse and may escalate and propagate through the mixture, causing coherent energy release. The propagating pressure pulse (which steepens to form a shock wave) has two main effects. Firstly, it collapses the vapour blanket, initiating rapid heat transfer. Secondly, it causes differential acceleration of the melt and water, which in turn leads to relative velocity breakup of the melt and a large increase in the melt surface area. As the energy of the melt is rapidly transferred to the water high pressure steam is produced, which expands, with the potential to cause damage to any surrounding structures.

In earlier work we have developed a mathematical model, called CHYMES, of the mixing stage [4,5,6] and are in a position to predict what type of mixtures are formed in many different situations. In a previous paper [7] we presented our new mathematical model of detonations, called CULDESAC. In this paper we present two extensions to this model. The first of these gives us the ability to study the effect of allowing for the presence of a permanent gas in the mixture. Permanent gases, such as hydrogen and argon, are often present in coarse mixture. Hydrogen is produced by dissociation of water at high temperatures and oxidation of metallic melts [8] and argon may be present in the mixture in some circumstances because of the thermite process used to generate high temperature melts [9]. The second modification allows us to switch between using a fast-running approximate Equation of State (EOS) for water to using computerized steam tables, e.g. the CEGB steam table package [10]. The latter are not ideal because their range of validity is too small for all detonation calculations but they do allow us to check the validity of our approximation in some circumstances.

In section 2 of this paper we describe the partial differential equations which make up the model and the constitutive relations used to close it. In section 3 we describe the solution procedure and in section 4 we describe the results from some example calculations. Finally, in section 5 we draw some conclusions.

2 Description of the Model

In this section we describe the partial differential equations and constitutive relations which constitute the model. The model is transient and one-dimensional (although this

may be planar, cylindrical, spherical or any user-specified slowly varying shape). We treat the mixture as consisting of melt particles, a permanent gas, water and steam. Behind the detonation front the particles are fragmented by boundary layer stripping and the water is heated by energy transfer from the fragments. This situation is shown schematically in figure 1. In the model we represent this situation using four different components, namely melt droplets (m), melt fragments (f), gas (g) and water (w).

Since the water is rapidly heated to supercritical pressures and temperatures we make the simplifying assumption that when distinct phases exist the steam and water are in thermal and mechanical equilibrium. We also assume that the melt fragment, water and permanent gas species are in mechanical equilibrium, which is reasonable since the melt fragments are very small ($\sim 100\mu m$) [11] and the permanent gas probably exists as small bubbles in the water. We assume that the fragmentation process is boundary layer stripping [12], although the model is sufficiently general to apply to any hydrodynamic fragmentation process. We have formulated this problem mathematically using the usual multiphase flow equations, where the presence of each species is specified by a volume fraction and all the species are at a common pressure. We make the simplifying assumption that the melt and fragments are incompressible, so that $\rho_f = \rho_m = constant$. Also since the water, the fragments and the gas are assumed to have the same velocity we set $V_f = V_w$ and $V_g = V_w$.

2.1 Conservation Equations

Conservation of mass applied to the water, gas, melt and fragments gives:

$$\frac{\partial}{\partial t}(\alpha_w \rho_w) + \frac{1}{A}\frac{\partial}{\partial x}(A\alpha_w \rho_w V_w) = 0, \tag{1}$$

$$\frac{\partial}{\partial t}(\alpha_g \rho_g) + \frac{1}{A}\frac{\partial}{\partial x}(A\alpha_g \rho_g V_w) = 0, \tag{2}$$

$$\frac{\partial}{\partial t}(\alpha_m \rho_m) + \frac{1}{A}\frac{\partial}{\partial x}(A\alpha_m \rho_m V_m) = -\Gamma_f, \tag{3}$$

and

$$\frac{\partial}{\partial t}(\alpha_f \rho_m) + \frac{1}{A}\frac{\partial}{\partial x}(A\alpha_f \rho_m V_w) = \Gamma_f. \tag{4}$$

In equations (3) and (4) Γ_f is the mass transfer rate due to fragmentation and is specified later.

Conservation of momentum for the melt and effective fluid, consisting of the water, the gas and the fragments, gives

$$\frac{\partial}{\partial t}(\alpha_m \rho_m V_m) + \frac{1}{A}\frac{\partial}{\partial x}(A\alpha_m \rho_m V_m^2) =$$

$$-\alpha_m \frac{\partial p}{\partial x} + K_{mw}(V_w - V_m) - \Gamma_f V_m \tag{5}$$

and

$$\frac{\partial}{\partial t}((\alpha_w \rho_w + \alpha_f \rho_m + \alpha_g \rho_g)V_w) + \frac{1}{A}\frac{\partial}{\partial x}(A(\alpha_w \rho_w + \alpha_f \rho_m + \alpha_g \rho_g)V_w^2) =$$

$$-(\alpha_w + \alpha_f + \alpha_g)\frac{\partial p}{\partial x} + K_{mw}(V_m - V_w) + \Gamma_f V_m. \tag{6}$$

The terms on the RHS of equations (5) and (6) represent the effect of the pressure gradient force, drag between the melt particles and an effective fluid (consisting of the water, gas and fragments) and momentum transfer due to mass transfer. Viscous forces have been ignored, since they are always negligible in situations of interest to us.

We also have an energy equation for each species. It is convenient to work in terms of the stagnation energy, defined by $e_s = e+(V^2/2)$ and the stagnation enthalpy defined by $h_s = e_s + p/\rho$. Conservation of energy for the melt, fragments, water and gas gives:

$$\frac{\partial}{\partial t}(\alpha_m \rho_m e_{sm}) + \frac{1}{A}\frac{\partial}{\partial x}(A\alpha_m \rho_m V_m h_{sm})$$
$$= -p\frac{\partial \alpha_m}{\partial t} + R_{mw}(T_w - T_m) + V_m K_{mw}(V_w - V_m) - \Gamma_f h_{sm}, \tag{7}$$

$$\frac{\partial}{\partial t}(\alpha_f \rho_m e_{sf}) + \frac{1}{A}\frac{\partial}{\partial x}(A\alpha_f \rho_m V_w h_{sf})$$
$$= -p\frac{\partial \alpha_f}{\partial t} + R_{fw}(T_w - T_f) + \Gamma_f h_{sm}, \tag{8}$$

$$\frac{\partial}{\partial t}(\alpha_w \rho_w e_{sw}) + \frac{1}{A}\frac{\partial}{\partial x}(A\alpha_w \rho_w V_w h_{sw})$$
$$= -p\frac{\partial \alpha_w}{\partial t} + R_{mw}(T_m - T_w) + R_{fw}(T_f - T_w) + R_{gw}(T_g - T_w)$$
$$+V_w K_{mw}(V_m - V_w) + K_{mw}(V_w - V_m)^2, \tag{9}$$

and

$$\frac{\partial}{\partial t}(\alpha_g \rho_g e_{sg}) + \frac{1}{A}\frac{\partial}{\partial x}(A\alpha_g \rho_g V_g h_{sg})$$
$$= -p\frac{\partial \alpha_g}{\partial t} + R_{gw}(T_w - T_g). \tag{10}$$

In the above equations the terms involving R_{mw} etc. represent thermal equilibration and the terms containing K_{mw} are the drag work. We have assumed that all the irreversible drag work heats up the water. A detailed derivation of these equations is given elsewhere [13].

We also have an equation for the length-scale of the melt droplets, given by:

$$\frac{\partial}{\partial t}(\alpha_m \rho_m L_m) + \frac{1}{A}\frac{\partial}{\partial x}(A\alpha_m \rho_m V_m L_m) = -\Gamma_f L_m - \Gamma_{frag}. \tag{11}$$

In the above equation the term involving Γ_f is due to mass transfer (it is a consequence of writing the transport equation in conservation form) and the term $-\Gamma_{frag}$ models the chosen fragmentation process.

In addition to the above equations we have the constraint that

$$\alpha_m + \alpha_f + \alpha_w + \alpha_g = 1. \tag{12}$$

This completes the specification of the differential equations. In the next subsections we will describe the constitutive relations, the Equations of State (EOS) and the boundary and initial conditions.

2.2 Constitutive Relations

In this section we describe the constitutive relations for drag, heat transfer and fragmentation currently employed in the model. These may be changed very easily as improved data becomes available.

2.2.1 Momentum Exchange

If the volume fraction of droplets is α_m there are $6\alpha_m/\pi L_m^3$ spherical droplets per unit volume. The drag force on a single droplet may be written as

$$F_D = \frac{1}{2} c_d \rho_e \pi \frac{L_m^2}{4} |V_w - V_m|(V_w - V_m) \tag{13}$$

where $\rho_e = (\alpha_w \rho_w + \alpha_f \rho_f + \alpha_g \rho_g)/(\alpha_w + \alpha_f + \alpha_g)$ is the effective density of the fluid dragging the melt drops. Thus the total drag force is

$$F_T = \frac{3}{4} \frac{c_d}{L_m} \rho_e \alpha_m |V_w - V_m|(V_w - V_m) \tag{14}$$

and comparison of equation (14) with equation (5) shows that

$$K_{mw} = \frac{3}{4} c_d \alpha_m \frac{\rho_e}{L_m} |V_w - V_m| \tag{15}$$

In the present work we have used a constant value of $c_d = 2.5$. This value is higher than the usual value of 0.4 to account for the increased drag when drops are fragmenting [12]. It is a simple matter to make c_d a function of the volume fractions etc., if required.

2.2.2 Heat Transfer

If the heat transfer rate is specified as the product of a heat transfer coefficient and the temperature difference it is easily shown that

$$R_{mw} = 6\alpha_m \frac{h_{mw}}{L_m}, \tag{16}$$

$$R_{fw} = 6\alpha_f \frac{h_{fw}}{L_f} \tag{17}$$

and

$$R_{gw} = 6\alpha_g \frac{h_{gw}}{L_g} \tag{18}$$

where h_{mw} is the heat transfer coefficient between the melt and water etc. and L_f is the fragment size. The heat transfer mechanisms between the melt and water are very complex and clearly depend on the time-history of each particle. The only experimental data available is rather crude and consists of time-averaged heat transfer coefficients for the duration of the fragmentation process [14]. Thus in the present model we have decided to choose constant values for the heat transfer coefficients. A value of $h_{mw} = 10^3\ W/m^2K$ was used for the melt when it was surrounded by a vapour film. This is a typical value obtained from a combination of radiation and film boiling [14]. This

value was increased by typically four orders of magnitude when vapour film collapse was judged to have occurred.

The treatment of vapour film collapse used here was simply to increase the heat transfer coefficient when the pressure exceeded a certain value, since this models pressure induced vapour film collapse. Because of the high initial temperature of the melt ($\sim 2500K$) in situations of interest to us, temperature controlled vapour film collapse was not considered to be important [15]. We have performed scoping calculations which show that the exact criterion for vapour film collapse is unimportant, since increasing the heat transfer rate between the large particles and the water only changes the solution by a small amount. This is because the heat transfer surface area of the large melt particles is very small compared with that of the fragments.

The fragment size L_f is not determined by the fragmentation model currently employed (see section 2.2.3) and was specified by reference to experimental data. A typical value of $L_f = 100\mu m$ was used [11]. Similarly, the size of the gas bubbles is not known, but this data is only needed in the heat transfer calculation and so it can be combined with the uncertainty in h_{gw}.

2.2.3 Fragmentation Model

As already mentioned we have chosen to use a boundary layer stripping model for fragmentation as this is thought to be the most appropriate for the study of vapour explosions [16]. We have used the model proposed by Carachalios et al. [16], who suggest that the stripping rate from a single fragment is given by

$$\frac{dm}{dt} = c_{frag}|V_m - V_w|\pi L_m^2\sqrt{\rho_m \rho_e} \tag{19}$$

where the empirical constant c_{frag} takes a value of approximately 1/6. Multiplying equation (19) by the number of drops per unit volume and comparing the result with equation (3) gives

$$\Gamma_f = \alpha_m c_{frag}|V_m - V_w|\sqrt{\rho_e \rho_m}/L_m \tag{20}$$

where all the constant terms have now been included in c_{frag}, so that $c_{frag} \sim 1$. Thus the mass stripping rate is proportional to the relative velocity and the square root of the effective density. As fragmentation occurs, the density of the surrounding fluid is increased by the addition of fragments and thus the fluid has more inertia to fragment the drops further.

The length-scale of the droplets is changed by the mass loss due to boundary layer stripping. For spherical drops it is easily shown that the mass loss rate given in equation (20) implies a length-scale source term of

$$\Gamma_{frag} = \frac{1}{3}\Gamma_f L_m \tag{21}$$

which is not surprising, as equation (21) implies that a droplets length-scale changes at one third the rate of its volume. We have also added an empirical function of our own to ensure that breakup only occurs for Weber numbers above a critical value ($We_{crit} \approx 12$). Details are given in reference 17.

It is interesting to note that the fragmentation model of Carachalios et al. is consistent with the data of Reinecke and Waldman [18] for the fragmentation of water droplets in air. They fitted their data by a fragmentation rate which varies proportional to $cos(\pi t^*/t^*_B)$ where $t^* = \frac{tU}{L}\sqrt{\frac{\rho_m}{\rho_w}}$ is the usual dimensionless time and t^*_B is the dimensionless fragmentation time. We note that the correlation of Carachalios et al. approximates the correlation of Reinecke and Waldman by a constant fragmentation rate, which is the time average of that of R&W for a breakup time of $t^*_B = 1$, (which is consistent with the spread in fragmentation data [12]).

2.3 Equations of State

The melt equation of state is very easy. We assume the melt to be incompressible so that $\rho_m = \rho_f =$ constant and to have a simple caloric equation of state so that $E_m = c_{vm}T_m$ and $E_f = c_{vm}T_f$. The gas is treated as a perfect gas, so that $p = (\gamma - 1)c_{vg}\rho_g T_g$ and $e_g = c_{vg}T_g$.

The EOS for water is more complicated and there is virtually no thermodynamic data on the properties of water at very high temperature and pressures. In our previous study [7] we used an approximate EOS (of the Grüneisen form) outside of the two-phase region. In this paper we compare some of our previous results with those obtained using a more accurate EOS. We have coded an option to allow us to use either the approximate EOS or the CEGB standard steam tables which are based on a fit to the free energy [10]. These tables are limited to pressures below 300MPa and temperatures below 1200K. The solution procedure requires that the EOS provides a means of calculating p and T, given ρ and e. However, the free energy is a function of ρ and T. Thus it was necessary to develop an iteration scheme which allows the user to guess a temperature and iterate until the internal energy predicted by the steam tables agrees with that produced by the code. Convergence is achieved relatively cheaply by predicting a new temperature, as follows:

$$T^n = T^o + (e^n - e^o)/c_{vw} \tag{22}$$

and then using the secant method to obtain the convergence to the required degree of accuracy.

Inside the two-phase region we used the lever-rule, as before [7].

2.4 Boundary and Initial Conditions

We are interested in solving the above equations in a closed vessel. Thus the only boundary condition needed is to set the velocities to zero at the vessel walls.

Initially, the volume fractions, void fraction, velocity and particle size distribution are specified. To simulate triggering some of the melt is fragmented in a small region of the solution domain. This causes a high heat transfer rate in these cells, the pressure rises locally and a detonation wave may develop.

3 Solution Procedure

We solve the partial differential equations using a finite difference method which employs the usual staggered grid arrangement. All convective terms are modelled using

upwind differencing for stability. As far as possible we use explicit methods, where appropriate treating source terms implicitly, to ensure that positive quantities remain positive [19]. A full description of the solution procedure is given elsewhere [13]. In this section we will describe the complications introduced by having two compressible species, namely the gas and water. The much simpler solution procedure which was used when only one compressible species was present is described in reference 7.

1. Equations (1), (2), (3) and (4) are used to time advance $\alpha_w\rho_w$, $\alpha_g\rho_g$, α_m and α_f, respectively.

2. Equations (5) and (6) are used to obtain the new velocity fields. The drag and mass transfer terms are treated implicitly and the convection and pressure gradient terms are treated explicitly. Thus at each point a 2×2 matrix is inverted to obtain both velocities simultaneously. This practice has proved to be very stable.

3. The new stagnation energies are found by time advancing the four equations (7) $\rightarrow$ (10). Using the stagnation form ensures that the Rankine-Hugoniot equation can be built into the solution scheme to give it good shock-capturing properties. The new velocity field is then used to determine the new internal energies. Because we have more than one compressible species it is not possible to determine the new volume fraction fields for the water and gas before the energy equation is solved. Thus at this stage we cannot form an accurate expression for $\frac{\partial\alpha}{\partial t}$ for use in the pressure-work terms. Instead we use a backward difference approximation for these terms. This means that at this stage energy is not conserved and we must correct the energy within the procedure which is used to determine the volume fractions and the pressure.

4. The caloric equations are used to determine the new melt and fragment temperature. It now remains to determine the pressure, the volume fractions of the water and gas and the temperature of the water and gas. Because the gas has a simple EOS we are able to produce a rapidly converging solution procedure as follows. Let X be a guess for the water volume fraction, then equation (12) can be used to construct the following equation for X,

$$X + \frac{(\alpha\rho)_g(\gamma-1)e_g}{p\left((\alpha\rho)_w/X, e_w\right)} = 1 - \alpha_m - \alpha_f. \tag{23}$$

This equation is used to obtain the new volume fraction for the water and then the remaining unknown quantities are easily derived. During the iteration process used to solve equation (23) the internal energies of the gas and water are updated, as shown below (for the gas species),

$$e_g^{new} = e_g^{old} + p^o(\alpha_g^{old} - \alpha_g^o) - p^o(\alpha_g^{new} - \alpha_g^o), \tag{24}$$

where the superscript o refers to the converged value at the previous time-step and the superscripts *old* and *new* refer to the old and new approximations at the new time level. Care has to be taken to ensure that during the course of the iteration procedure unphysical values are not obtained. We solved the above equation using the bisection method. An upper bound on X is easily obtained,

since $X_{max} = 1 - \alpha_m - \alpha_f$. Because the time-step is relatively short the converged value at the old time provides a good estimate of the solution. We used the bisection method applied to a small range either side of this value, subject to the constraint on X_{max} above. This procedure was found to be robust and the correction procedure applied to the pressure-work terms ensured that energy conservation was extremely good.

This completes a cycle of the solution procedure. The new solution procedure requires approximately twice as much CPU time per time-step compared with that for the case of no gas present.

4 Example Simulations

The model has been thoroughly tested as it has been developed (see reference 7 for details) and has been used to study melt-water detonations [7]. In the next sections we will describe a test problems which we have used to study the effect of changing the water EOS and of adding permanent gas. However, before doing this we will present some results for the propagation of sound waves in gas/water mixtures. These calculations were performed in order to check that the code was working correctly. The sound speed was determined by performing calculations where a small (0.1% peak amplitude) cosine variation was made to the pressure about a uniform initial state (p=0.1MPa, T=300K). By monitoring the pressure at a fixed point it is possible to determine the period of the motion and hence to determine the speed of sound. The results were compared with the theory of Campbell and Pitcher [20] and found to be in very good agreement. Table 1 shows typical values from this comparison exercise.

Gas Fraction	Code Prediction	Theory
-	(m/s)	(m/s)
0.0	1463	1483
0.001	313	316
0.01	100	101

Table 1: Comparison of the predicted and calculated sound speeds

4.1 Description of the Calculations

In this section we describe the parameters and initial conditions used in the simulations. Table 2 contains a list of all the parameters not specified in the earlier sections. All the simulations were started by assuming that there was a spatially uniform mixture with a specified melt volume fraction and void fraction. The gas to water heat transfer rate was chosen to be sufficiently high so that the gas and water remained in thermal equilibrium ($h_{gw} = 10^3\ W/m^2K, L_g = 10\mu m$). This approximation should be valid if the gas bubbles are very small, as they are for dissolved gases. This mixture was assumed to be at rest. An explosion was triggered by instantaneously fragmenting 90% of the melt in the first 0.01m adjacent to the right-hand wall.

Parameter	Value	unit
Time-step	2×10^{-8}	s
Space-step	0.005	m
Initial particle size	0.005	m
Initial pressure	0.1	MPa
Heat transfer rate - vapour blanketed	10^3	W/m^2K
Heat transfer rate - liquid-liquid contact	10^7	W/m^2K
Pressure required to collapse vapour blanket	0.2	MPa
Initial melt temperature	2500	K
Melt density	7000	kg/m^3
Melt heat capacity	500	J/kgK
Melt surface tension	0.4	N/m
Initial melt volume fraction	0.1	-
Heat capacity of gas	300	J/kgK
Ratio of specify heats for gas	1.4	-

Table 2: Parameters used in the detonation simulations

4.2 The Effect of Changing the Water EOS

The effect of changing the EOS was examined by repeating some of the calculations reported in reference 7 using the new EOS. Figures 2 and 3 show the results of two such comparisons. The first corresponds to a comparison for the data given in Table 2 and the second figure corresponds to the same situation but with the fragment to water heat transfer rate reduced by a factor of 10. In the second comparison the calculation stopped prematurely because the pressure exceeded the maximum range of the steam table package. (In this case the pressure profile is very spiky and one of the spikes exceeded a pressure of 300MPa, causing the steam table package to stop internally.)

It is clear from this comparison that the approximate EOS is not significantly in error in the region of interest to us in detonation simulations. Use of the steam table EOS results in pressures and detonation velocities which are generally lower than those predicted using the approximate EOS but the difference is not significant and does not account for the difference between the predicted pressures and those observed in most steam explosion experiments, see e.g. [9]. Also the new EOS does not remove the very spiky nature of the pressure profiles which occurs for low heat transfer rates and/or low void fractions. Their origin is explained in reference 7 and the current work clearly establishes the fact that they are not caused by the approximate EOS used in our earlier work.

The steam table EOS has the disadvantage that it is not defined above certain pressures etc. and it is computationally much more expensive to use (run times are increased by a factor of 10 because of numerical differentiation performed within the steam table routines). Thus we will use the approximate EOS in the next subsection where we study the effect of adding a permanent gas.

4.3 The Effect of Adding a Permanent Gas

The simulation shown in Figure 3(a) was repeated with gas fractions of 0.1%, 1% and 5%. (The melt/coolant mass ratio was kept fixed in each case.) As expected, increasing the proportion of gas increased the effect of the gas. Figure 4 shows the pressure profile as a function of time for the 5% case. The figure shows that the peak pressures are reduced slightly and the detonation velocity is slightly lower than those for the case of no gas present. However, the effect is small and does not account for the difference between the predicted and experimentally measured pressures.

It is thought that if the peak pressures were reduced by other effects, such as allowing for thermal disequilibrium, then the effect of adding a permanent gas could be significant, as it is in the case of sound waves. This conjecture was tested by reducing the fragment to water heat transfer rate by a factor of 10 from that used in the simulation shown in Figure 4 and repeating the comparison for calculation with no gas and one with 5% gas. A comparison of the results is given in Figure 5. In this situation the peak pressures are reduced by almost a factor of two, showing that the effect of adding a gas does indeed become more important as the strength of the detonation is reduced. However, the pressures behind the detonation front are still only slightly reduced. Thus it would appear that the peak pressure must be reduced still further before the presence of a permanent gas has a significant affect on the behaviour of a detonation.

5 Conclusions

We have described a mathematical model of melt/water detonations. The usual multiphase flow equations are used to simulate the passage of a detonation wave through a mixture of melt and water. The model assumes that differential acceleration of the melt and water, by the passage of a shock front, causes relative velocity induced fragmentation of the melt. This fragmentation, together with the collapse of the vapour blanket, leads to the development of a detonation wave. In this work we do not fit a shock wave at the detonation front or assume steady-state propagation but calculate the response of the system given an initial disturbance. Thus we can examine the *development* of detonations from a simulated trigger.

In this paper we have presented new computational results obtained by using a steam table package instead of an approximate EOS and results from computations performed to study the effect of adding a permanent gas to the melt/water mixture. These results show that the approximate EOS used in our earlier work provides a useful, computationally efficient EOS which does not introduce a significant error in high pressure detonation calculations. We have observed that the presence of a permanent gas does not alter the predicted detonation velocities and peak pressures significantly, in the case of high pressure detonations. We have also observed that the effect increases as the strength of the detonation is decreased. We have checked that the code correctly reproduces well-known results for the reduction of the sound speed in gas/water mixtures. Thus it is conjectured that if detonation pressures were reduced by modelling other physical effects in the code, then the effect of permanent gases could be important.

The very large pressures predicted by CULDESAC are consistent with predictions of

other workers, e.g. [21] and with the results from the very occasional experiment which results in a very energetic explosion, e.g. experiment RC-2 at Sandia National Laboratory which gave rise to pressures of $\sim$ 100 MPa [22]. However, the predicted pressures are approximately an order of magnitude higher than most of those observed in experiments with high temperature simulant materials. There are a number of reasons for this. Firstly, it is virtually impossible to produce a homogeneous coarse mixture in most experimental arrangements. (This is not the case in stratified geometries, where highly repeatable initial conditions can set-up [23].) Thus 3d spatial inhomogeneities weaken detonation fronts and reduce the peak pressures. In highly voided systems it is likely that the melt and water are not located close to each other so that the mixture is very inhomogeneous on the scale of the width of the detonation front. Secondly, thermal disequilibrium in the water phase is known to be important [24]. All the water is not heated to a uniform temperature. Close to the fragments the water is heated extremely rapidly causing the pressure to rise. This induces a large subcooling in the unheated water and heat is then lost to this region from the heated water and the pressure is reduced. In the future, we hope to investigate these effects by making further developments to the CULDESAC model.

Acknowledgements

This work was funded by the General Nuclear Safety Research (GNSR) Programme. We would like to thank Dr. R.P. Anderson of ANL for a useful discussion on detonations which led to us examining the effect of the presence of a permanent gas.

References

[1] G. Long, *Explosions of molten metal in water - causes and prevention.* Metals progress, **71**, 107-112, (1957).

[2] S.A. Colgate and T. Sigurgeirsson, *Dynamic mixing of water and lava.* Nature, **244**, 552-555, (1973).

[3] A.W. Cronenberg, *Recent developments in the understanding of energetic molten fuel coolant interaction.* Nucl. Safety, **21**, 319-337, (1980).

[4] A. Thyagaraja and D.F. Fletcher, *Buoyancy-driven, transient, two-dimensional thermo-hydrodynamics of a melt-water-steam mixture.* Comput. Fluids, **16**, 59-80, (1988).

[5] D.F. Fletcher and A. Thyagaraja, *Numerical simulation of two-dimensional transient multiphase mixing.* Proc. 5th Int. Conf. on Numerical Methods in Thermal Problems, Montreal, Canada, June 29th - July 3rd 1987, **V**(2), 945-956, Pineridge, (1987).

[6] D.F. Fletcher and A. Thyagaraja, *A method of quantitatively describing a multi-component mixture.* PhysicoChem. Hydrodynam., **9**, 621-631, (1987).

[7] D.F. Fletcher and A. Thyagaraja, *A mathematical model of melt/water detonations.* Culham Laboratory Report: CLM-P842, (1988). (To appear in Applied Mathematical Modelling.)

[8] M.F. Young, M. Berman and L.T. Pong, *Hydrogen generation during fuel/coolant interactions.* Nucl. Sci. Eng., **98**, 1-15, (1988).

[9] M.J. Bird, *An experimental study of scaling in core melt/water interactions.* Paper presented at the 22nd National Heat Transfer Conference, Niagara Falls, August 5-8, 1988.

[10] M.C. Cullen, *CEGB Revised Steam Table Package - Pollack Formulation, Vol. 2 - Scientific Statement.* CEGB Report CC/P662, (1982).

[11] D.F. Fletcher, *The particle size distribution of solidified melt debris from molten fuel-coolant interaction experiments.* Nucl. Engng. Des., **105**, 313-319, (1988).

[12] M. Pilch and C.A. Erdman, *Use of breakup time data and velocity history data to predict the maximum size of stable fragments for acceleration-induced breakup of a liquid drop.* Int. J. Multiphase Flow, **13**, 741-757, (1987).

[13] D.F. Fletcher and A. Thyagaraja, *Multiphase flow simulations of shocks and detonations, Part I: Mathematical formulation and shocks.* Culham Laboratory Report:

CLM-R279, (1987).

[14] D.F. Fletcher, Modelling transient energy release from molten fuel coolant interaction debris. AEE Winfrith Report: AEEW-M2125, (1984).

[15] T.A. Dullforce, D.J. Buchanan and R.S. Peckover, *Self-triggering of small-scale fuel-coolant interactions: 1. experiments.* J. Phy. D. Appl. Phys., **9**, 1295-1303, (1976).

[16] C. Carachalios, M. Bürger and H. Unger, *A transient two-phase model to describe thermal detonations based on hydrodynamic fragmentation.* Proc. Int. Meeting on LWR severe accident evaluation, Cambridge, Massachusetts, 28 August - 1 September, (1983).

[17] D.F. Fletcher and A. Thyagaraja, *Multiphase flow simulations of shocks and detonations, Part III: Droplet laden gas flows.* Culham Laboratory Report: CLM-R283, (1988).

[18] W.G. Reinecke and G.D. Waldman, *An investigation of water droplet disintegration in the region behind strong shocks.* Presented at 3rd Int. Conf. on Rain Erosion and Related Phenomena, Hampshire, England, (1970).

[19] A. Thyagaraja, D.F. Fletcher and I. Cook, *One dimensional calculations of two-phase mixing flows.* Int. J. Numer. Methods Eng., **24**, 459-469, (1987).

[20] I.J. Campbell and A.S. Pitcher, *Shock waves in liquids containing gas bubbles.* Proc. Roy. Soc., **A243**, 534-545, (1958).

[21] C. Carachalios, M. Bürger and H. Unger, *Triggering and escalation behaviour of thermal detonations.* AIChE Symp. Series, **81**, 259-266, (1985).

[22] M. Berman, Light Water Reactor Safety Research Program Semiannual Report, October 1983 - March 1984, NUREG/CR-4459, (1986).

[23] R. Anderson, D. Armstrong, D. Cho and A. Kras, *Experimental and analytical study of vapour explosions in stratified geometries.* ANS Proc. 1988 National Heat Transfer Conf., Houston, July 24-27, 1988, **3**, 236-243, (1988).

[24] S.J. Board, R.B. Duffey and C.L. Farmer, *A non-equilibrium analysis of thermal explosions.* CEGB Rept. RD/B/N2186, (1972).

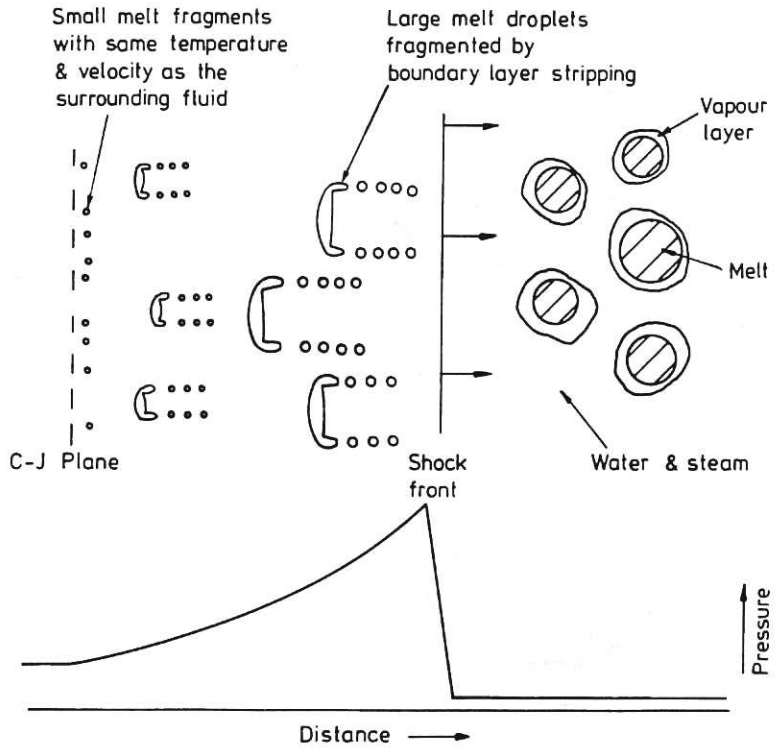

Fig. 1 Schematic Representation of a Detonation Front in a Melt/Water Mixture.

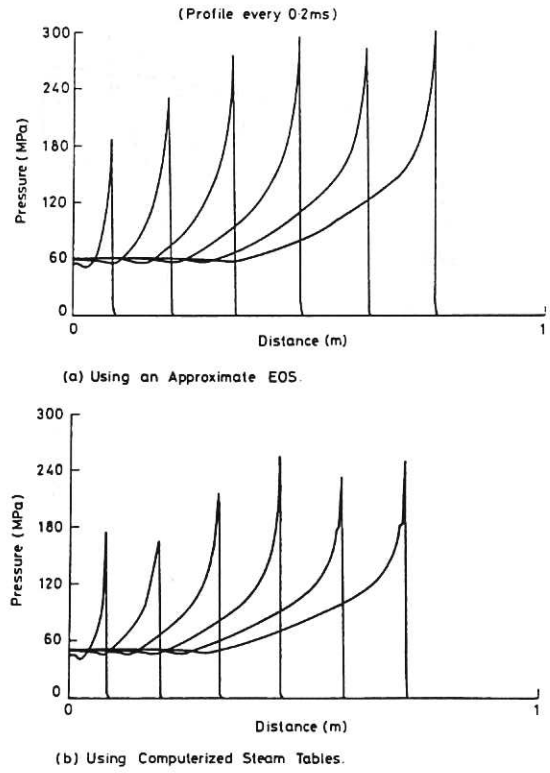

Fig. 2 A Comparison of the Development of the Pressure Profile for the $\alpha=0.7$, $h=10^7$ W/m^{2}K Case.

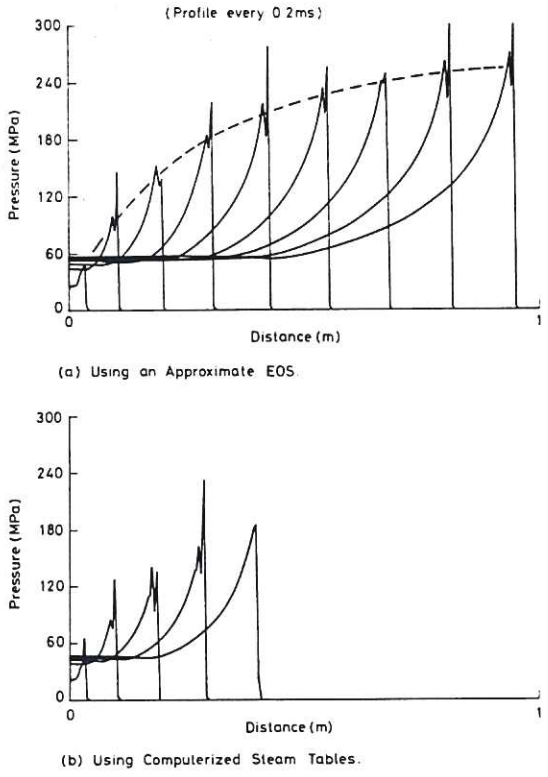

Fig. 3 A Comparison of the Development of the Pressure Profile for the $\alpha = 0.7$, $h = 10^6$ W/m^{2}K case.

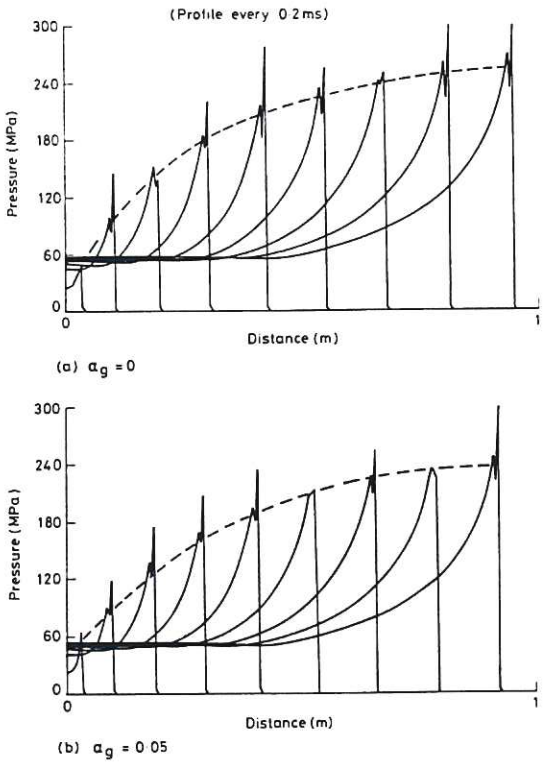

Fig. 4 The Effect of Adding Permanent Gas for a Simulation where $\alpha = 0.7$ and $h = 10^6$ W/m^{2}K.

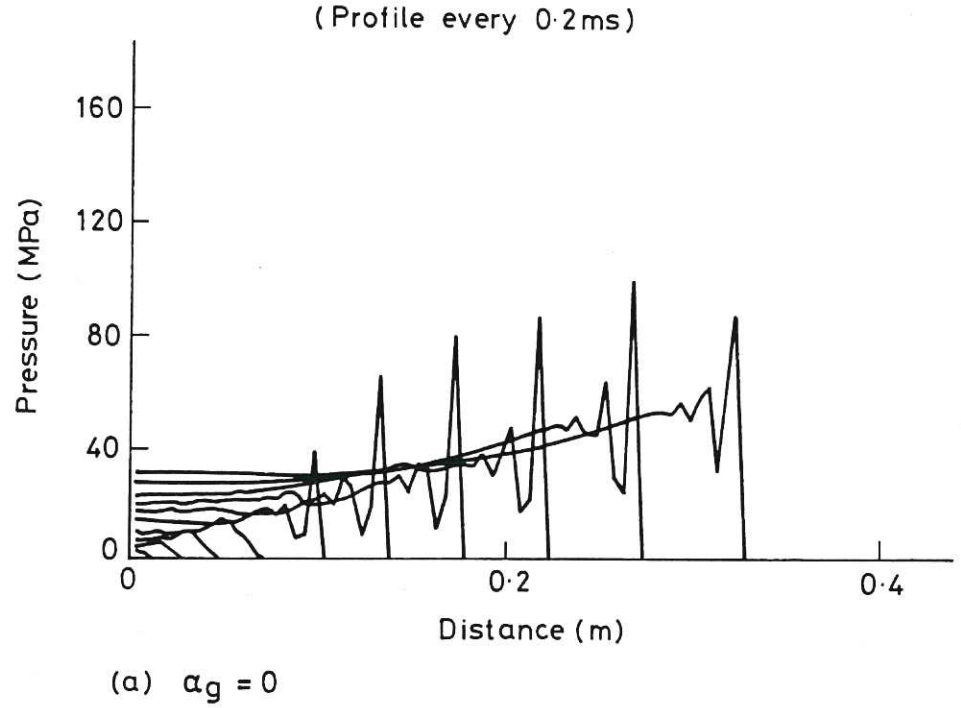

(a) $\alpha_g = 0$

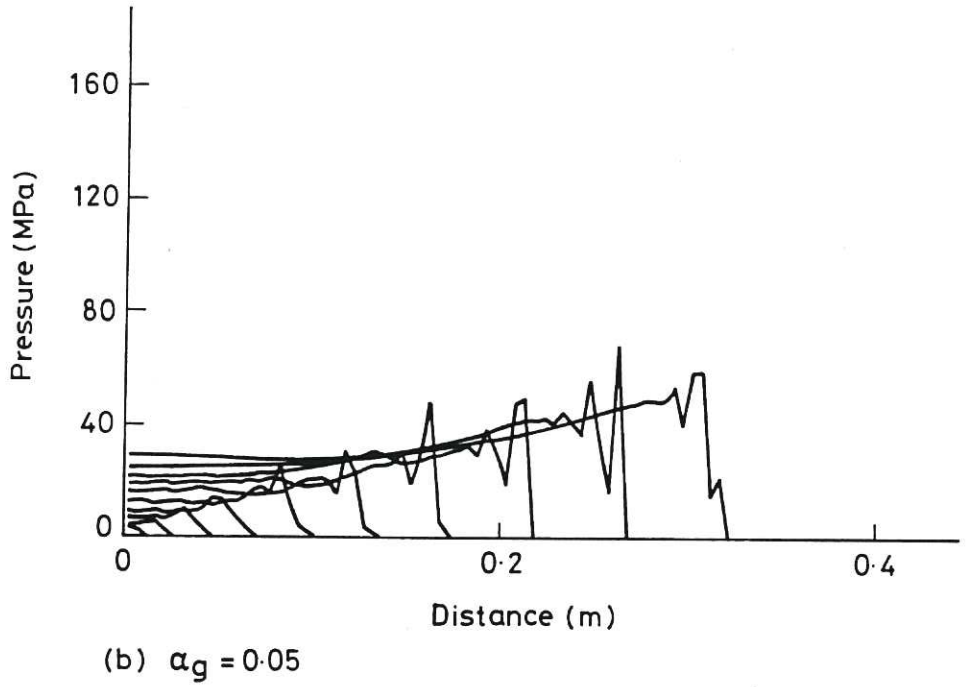

(b) $\alpha_g = 0{\cdot}05$

Fig. 5 The Effect of Adding Permanent Gas for a Simulation where $\alpha = 0.7$ and $h = 10^5 W/m^2K$.